JACS Au
AN OPEN ACCESS JOURNAL OF THE AMERICAN CHEMICAL SOCIETY

pubs.acs.org/jacsau

Article

Surfactant-free Synthesis of Spiky Hollow Ag−Au Nanostars with Chemically Exposed Surfaces for Enhanced Catalysis and Single-Particle SERS

Ziwei Ye,[‖] Chunchun Li,[‖] Maurizio Celentano, Matthew Lindley, Tamsin O'Reilly, Adam J. Greer, Yiming Huang, Christopher Hardacre, Sarah J. Haigh, Yikai Xu,* and Steven E. J. Bell*

Cite This: *JACS Au* 2022, 2, 178−187

Read Online

ACCESS | Metrics & More | Article Recommendations | Supporting Information

ABSTRACT: Spiky/hollow metal nanoparticles have applications across a broad range of fields. However, the current bottom-up methods for producing spiky/hollow metal nanoparticles rely heavily on the use of strongly adsorbing surfactant molecules, which is undesirable because these passivate the product particles' surfaces. Here we report a high-yield surfactant-free synthesis of spiky hollow Au−Ag nanostars (SHAANs). Each SHAAN is composed of >50 spikes attached to a hollow ca. 150 nm diameter cubic core, which makes SHAANs highly plasmonically and catalytically active. Moreover, the surfaces of SHAANs are chemically exposed, which gives them significantly enhanced functionality compared with their surfactant-capped counterparts, as demonstrated in surface-enhanced Raman spectroscopy (SERS) and catalysis. The chemical accessibility of the pristine SHAANs also allows the use of hydroxyethyl cellulose as a weakly bound stabilizing agent. This produces colloidal SHAANs that remain stable for >1 month while retaining the functionalities of the pristine particles and allows even single-particle SERS to be realized.

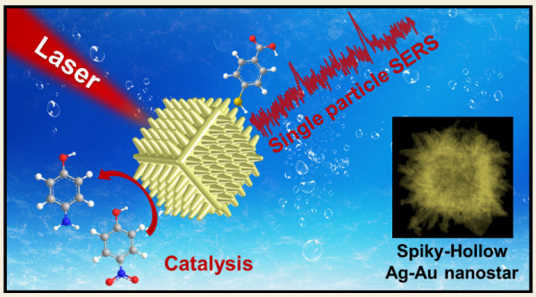

KEYWORDS: *spiky hollow Au−Ag nanostar, surfactant molecule, surface-enhanced Raman spectroscopy, hydroxyethyl cellulose, self-assembly*

INTRODUCTION

Ag and Au nanoparticles have been extensively studied in the past few decades due to their unique catalytic and plasmonic properties.[1−6] Up to now, the most popular route to produce Ag and Au nanomaterials has been through bottom-up colloidal synthesis, which typically employs a strongly adsorbing surfactant to direct particle growth and provide colloidal stability.[7−11] A variety of anisotropic metal nanoparticles with distinct properties can now be synthesized with the aid of surfactants, for instance, the polyvinylpyrrolidone (PVP)-assisted synthesis of nanocubes,[12−14] the cetyltrimethylammonium bromide (CTAB)-assisted synthesis of nanorods,[15−17] the Triton-X-assisted synthesis of nanostars, and so on.[18−20] Whereas the use of surfactant capping molecules offers easy manipulation of the morphology of the synthesized nanoparticles, their existence is also problematic for nearly every type of application, for example, in plasmonic sensing and catalysis, where the surface-bound surfactant molecules act as both physical and chemical barriers that restrict the free access of analytes/reactants to the nanosurface,[9,21−23] or in bioapplications where the free surfactants induce cytotoxicity.[24,25] As a result, methods for the postsynthesis removal of surfactant molecules or surfactant-free synthesis have become important areas of research.[26−30] For example, Gao et al. showed that diethylamine can be used as a general and highly effective intermediate ligand to facilitate the replacement of strongly adsorbed capping agents with weakly adsorbed capping agents.[29] Odom et al. demonstrated that it was possible to use weakly adsorbing and biocompatible Good's buffers, such as 4-(2-hydroxyethyl)-1-piperazineethanesulfonic acid, to synthesize Au nanostars.[30]

Among the anisotropic metal nanoparticles reported to date, spiky or hollow nanoparticles have drawn particular interest as catalysts due to their large surface-to-volume ratio and the presence of high-index crystal planes that are composed of highly active low-coordinated atoms.[31,32] If they are composed of plasmonic materials, such as Au and Ag, then spiky or hollow nanoparticles have also been shown to possess significantly enhanced plasmonic properties compared with their isotropic counterparts.[33−36] To take full advantage of the plasmonic and catalytic properties of hollow and spiky

Received: October 18, 2021
Published: December 16, 2021

https://doi.org/10.1021/jacsau.1c00462
JACS Au 2022, 2, 178−187

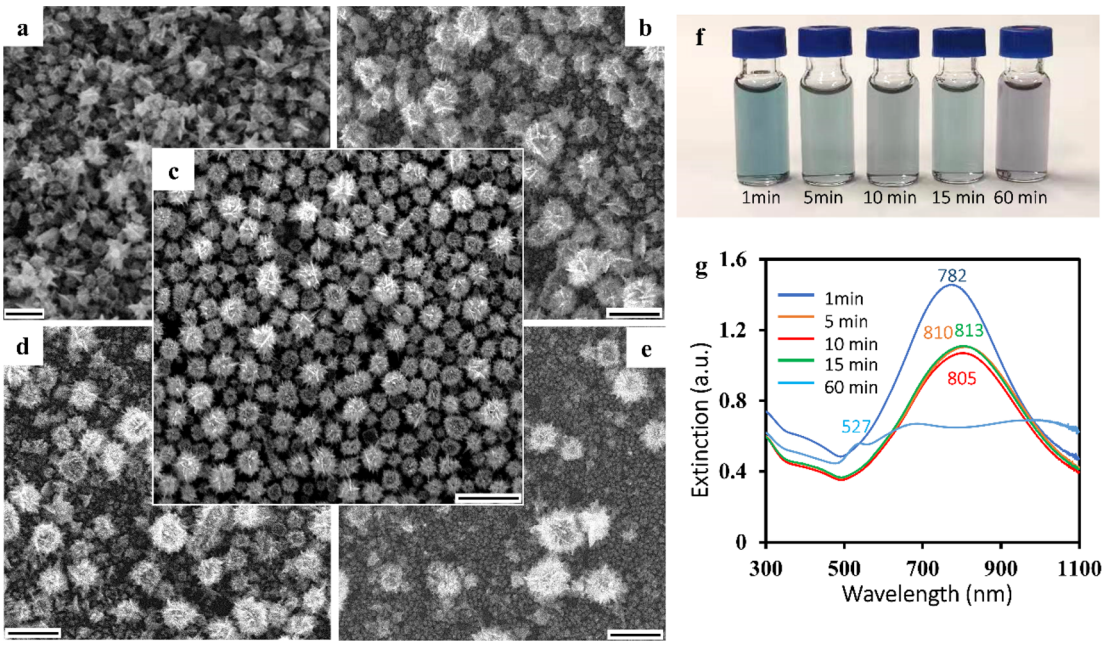

Figure 1. (a–e) Scanning electron microscopy (SEM) images of Au/Ag alloy nanoparticles synthesized by incubating the mixture solution of $HAuCl_4$, NaCl, and $AgNO_3$ for (a) 0, (b) 5, (c) 10, (d) 15, and (e) 60 min and then adding ascorbic acid. Scale bars in all images correspond to 500 nm. (f) Corresponding optical images of colloids prepared with different incubation times. (g) UV–vis spectra of colloids prepared with different incubation times.

nanoparticles, a few research groups have reported methods for synthesizing Au/Ag nanostars that are both spiky and hollow.[20,37−41] However, in general, bottom-up methods that allow the production of spiky Au/Ag nanostars that contain a hollow interior remain extremely rare. More importantly, the current methods for producing Ag/Au nanostars with hollow interiors are either complex or require the extensive use of surfactants, which has significantly limited the application of these particles, despite their promising properties. For example, Rodriguez-Fernández et al. showed that spiky and hollow Au nanoparticles with tailored near-infrared plasmonic properties could be produced using Triton X-100 as the growth-directing agent.[20] Evans et al. showed that spiky and hollow Au nanoparticles with excellent catalytic and surface-enhanced Raman spectroscopy (SERS) activity could be produced using methyl-orange-$FeCl_3$ templates.[38]

In this work, we demonstrate a mild and surfactant-free synthesis, which can be completed at room temperature within minutes to produce spiky hollow Au–Ag nanoparticles (SHAANs) with ca. 100% morphological yield. The unique morphology of the SHAANs combined with their highly accessible surfaces allows them to exhibit outstanding catalytic and single-particle SERS activities, which were significantly enhanced compared with those of their conventional surfactant-capped counterparts. Moreover, the high accessibility of the SHAAN surface also meant that they could be stabilized in the colloidal state using extremely weakly bound capping ligands, such as hydroxyethyl cellulose (HEC). This allowed the product colloid to remain stable for >1 month while fully retaining the surface accessibility of the particles. This is significant because good colloidal stability is crucial for a variety of important applications, such as catalysis, kinetic monitoring, and slow drug release,[1,42,43] but has typically been overlooked in previous studies regarding the surfactant-free synthesis of colloidal nanoparticles. More generally, the ability to access enhanced nanoproperties with anisotropic nanoparticles prepared using an easy and reliable room-temperature process not only offers a powerful tool for fundamental research but also paves the way for a broad range of important real-life applications, such as trace molecule detection, biomedical diagnostics, or the construction of functional devices.

RESULTS AND DISCUSSION

The synthesis of the SHAANs is a simple and rapid one-step process. In brief, NaCl and $AgNO_3$ solutions are first added in sequence to a $HAuCl_4$ solution under constant stirring. The mixture is then incubated, after which L-ascorbic acid solution is quickly injected. (See details in the Materials and Methods section of the Supporting Information.) This causes the color of the solution to change immediately (typically within ca. 15s), indicating the formation of the product nanoparticles. The critical step in the process is the incubation of the mixed $HAuCl_4$, NaCl, and $AgNO_3$ solution before the addition of L-ascorbic acid. As shown in Figure 1a–e, the morphology of the nanoparticles obtained changed dramatically with different incubation times. The addition of ascorbic acid without incubation produced small spiky nanoparticles with an average diameter of ca. 40 nm. The resulting colloid had a light-blue color with λ_{max} measured via UV–vis at ca. 782 nm (Figure 1f,g). Further scanning transmission electron microscopy (STEM) characterization and energy-dispersive X-ray (EDX) spectroscopy of this colloid sample revealed that some of the nanoparticles that appeared to have a hollow interior when observed with scanning electron microscopy (SEM) actually had a Ag/AgCl core (Figure S1). As shown in Figure 1b, when the incubation time was extended to 5 min, approximately half of the nanoparticles became larger SHAANs with a particle diameter of ca. 150 nm. These SHAANs had a larger number of spikes on the surface compared with smaller nanoparticles obtained with less incubation, and the spikes were notably

https://doi.org/10.1021/jacsau.1c00462
JACS Au 2022, 2, 178–187

narrower and longer. Additionally, the interiors of particles were found to be hollow, which will be discussed in detail in the following section. The change in morphology with incubation was also reflected in the color of the colloids and their UV−vis extinction spectra. As shown in Figure 1f,g, the color of the colloids with incubation was clearly different, and their extinction peaks were broadened and red-shifted significantly compared with the nonincubated sample. The optimal incubation time, which led to the highest yield (ca. 100% morphological yield) of SHAANs, was found to be 10 min, as shown in Figure 1c. The resulting colloid was gray, with its UV−vis extinction peak centered around 805 nm (Figure 1f,g). Extending the incubation time beyond 10 min led to the population of SHAANs decreasing and eventually nearly completely disappearing. As shown in Figure 1d, the population of the product colloid with 15 min of incubation was similar to those obtained with 5 min of incubation, which is reflected by their identical colors and UV−vis extinctions (Figure 1f,g). If the incubation time was increased to 60 min, then very few SHAANs were formed, and the product colloid mainly consisted of small (ca. 30 nm) spheres (Figure 1e). Unsurprisingly, this colloid was purple, with a UV−vis extinction centered at ca. 527 nm (Figure 1f,g), which is characteristic of small spherical Au nanoparticles.[44]

Further characterization of the nanoparticles was performed by scanning transmission electron microscopy−high-angle annular dark field (STEM-HAADF) imaging. This was used in combination with energy-dispersive X-ray spectroscopy (EDX) to investigate the internal morphology, local elemental distribution, and composition of the SHAANs. Images from the 10 min incubated specimen revealed that the homogeneous population of nanoparticles has cubic hollow cores in addition to the spiky surface morphology observed by SEM (Figure 2a). The average diameter of the cubic core was found to be 150 ± 16 nm, as measured from 100 individual SHAANs. Figure 2b shows the high-magnification STEM-HAADF image of a typical SHAAN. The hollow cavity of the SHAAN was measured to be ca. 100 nm in diameter, and the length of spikes ranged between 30 and 45 nm. Elemental mapping revealed a fairly evenly dispersed mixture of Ag and Au, which resembled bimetallic Au−Ag alloys, with a mean composition of 90 at % Au and 10 at % Ag (Figure 2c,d). Interestingly, as shown in Figure 2e,f, the high-magnification elemental line scan also revealed that the at % ratio between Ag and Au was clearly higher at the surface of the SHAANs, which suggested the existence of a ∼1 nm thick Ag-rich surface layer that could have been formed due to the lower surface energy of Ag compared with Au.[45] STEM-HAADF analysis for a non-incubated specimen (see Figure S2) also revealed some hollow particles but with a smaller and less regular size and shorter spikes, consistent with the SEM data. These particles also had a composition of 90 at % Au and 10 at % Ag and a few nanometers thick Ag-rich surface layer (Figures S3 and S4).

The proposed mechanism for the formation of SHAANs is shown in Scheme 1. The synthesis is initiated by the addition of $AgNO_3$ to a mixed $NaCl/HAuCl_4$ solution, which leads to the formation of small AgCl seed nanoparticles. This is consistent with the observation that the mixture solution gradually changes from transparent to slightly cloudy after the addition of $AgNO_3$. Subsequent incubation leads to the growth of the AgCl seeds to form larger cubic AgCl nanoparticles; however, this process can be interrupted by the addition of ascorbic acid, which triggers a series of redox reactions (Table S1) that ultimately lead to the formation of SHAANs if the optimized incubation time of 10 min is used. More specifically, the addition of ascorbic acid to the incubated solution leads to the reduction of the AgCl nanoparticles to Ag^0 nanoparticles, as has been previously observed.[46−48] However, these are not stable in the presence of Au^{3+} cations, which can galvanically reduce them, leading to the replacement of the Ag^0 by Au^0 in the nanocrystal structure, a process that would be expected to yield cubic hollow Au shells.[46,47] Simultaneously, the presence of ascorbic acid and Au^{3+} cations along with residual Ag^+ and Cl^- leads to growth of spikes on the surface of the particles.[34]

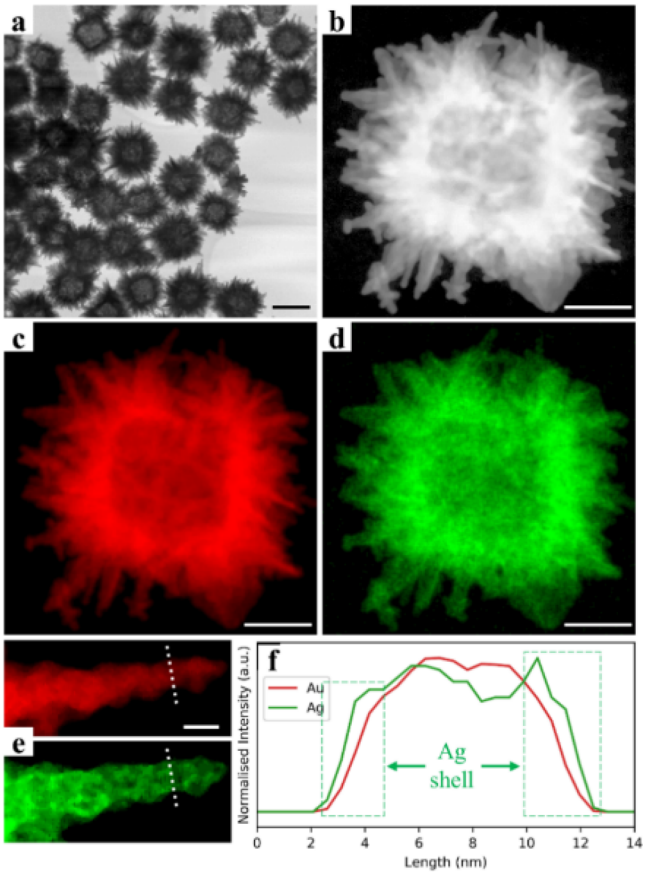

Figure 2. (a) Low- and (b) high-magnification scanning transmission electron microscopy−high-angle annular dark field (STEM-HAADF) images of SHAANs. Energy-dispersive X-ray (EDX) elemental mapping of SHAANs: (c) Au mapping image and (d) Ag mapping image. (e) EDX elemental mapping of a tip on the SHAAN shown in panel b. (f) Plot showing the material composition obtained with a high-magnification elemental line scan across the line labeled in panel e. Scale bars in panel a, panels b−d, and panel e correspond to 200, 60, and 10 nm, respectively.

This mechanism accounts for the importance of the duration of the incubation step and the nature of the products that are formed when it is changed from the optimum value. If the initial mixture was over-incubated (60 min), then the majority of Ag^+ and Cl^- ions were consumed in the growth of AgCl nanoparticles, and not enough were left to assist the formation of Au spikes. Therefore, the nanoparticles formed by the subsequent addition of ascorbic acid were mostly quasi-spherical (Figure 1e). In contrast, if the initial mixture was under-incubated (0 min), then there were not sufficient AgCl seeds to template the growth of SHAANs, and the AgCl seeds that were available were under-grown, which resulted in the

https://doi.org/10.1021/jacsau.1c00462
JACS Au 2022, 2, 178−187

Scheme 1. Schematic Illustration of the Formation of SHAANs with 10 min of Incubation Time Compared with When a 0 min of Incubation Is Used[a]

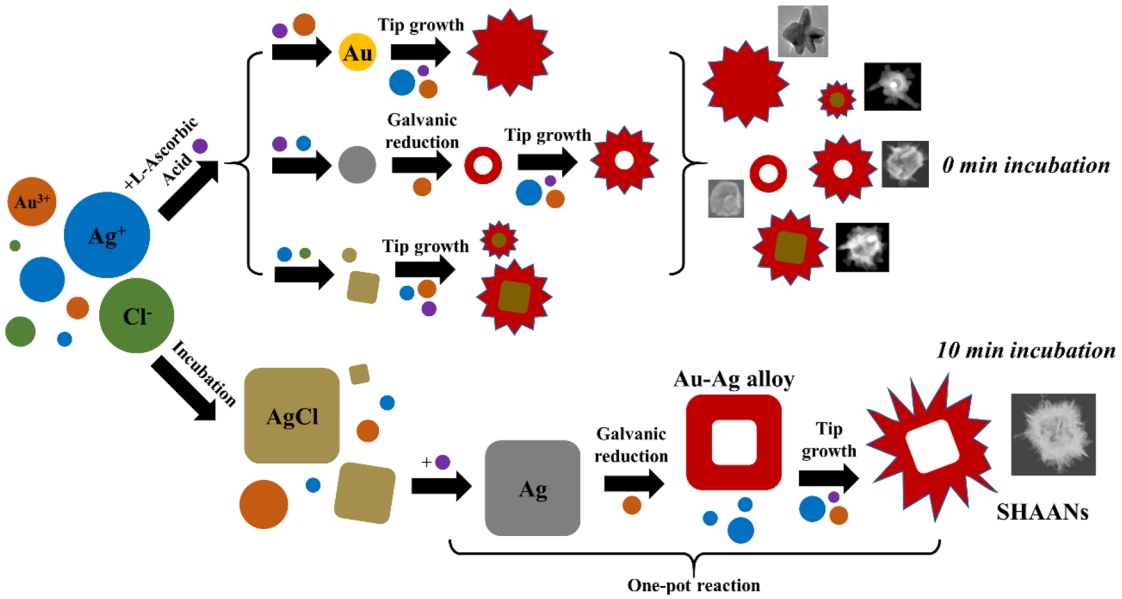

[a]Without incubation, the reaction goes through three simultaneous pathways, which leads to the formation of a mixture of nanoparticles including solid Au stars, Au hollow spheres, hollow Ag−Au stars, and solid Au stars with spherical/cubic AgCl cores. With 10 min of incubation, the reaction goes through a single pathway, leading to the formation of SHAANs.

formation of polydisperse spiky/hollow nanoparticles (Figure 1a and Figure S2). Although it is important to use the correct incubation time to achieve an appropriate balance between AgCl seeds, Ag^+ and Cl^- necessary for the formation of SHAANs (Figure 1c), it is useful to stress that provided that this time is used, the process is very robust, and it reliably generates SHAANs, as shown by SEM and SERS measurements in Figures S5 and S6. Although AgCl nanoparticles act as intermediates during the synthesis, a significant amount of residual AgCl is not expected to be present in the product SHAANs because it is reduced by the excess ascorbic acid in the solution. This was confirmed by the observation that washing SHAANs with ammonia−water, which would dissolve any residual AgCl, gave no detectable change in the morphology of the SHAANs (Figure S7).

X-ray photoelectron spectroscopy (XPS) was used to further study the surface composition of the SHAANs, in particular, to identify the oxidation state of the metals and the number of species present. Surprisingly, the XPS revealed that Ag was present in just one oxidation state, Ag^+, indicated by the photoelectron peak at 367.5 eV (Ag $3d_{5/2}$) (Figure 3a).[49,50] Because, as previously discussed, it is unlikely that a significant amount of AgCl is present in the product SHAANs, the Ag^+ observed by XPS is most likely in the form of Ag_2O, which is formed postsynthesis due to the high reactivity of colloidal Ag toward oxygen.[51] As shown in Figure 3b, the XPS also showed a photoelectron peak at 83.4 eV, corresponding to metallic Au $4f_{7/2}$. Interestingly, the binding energy observed for Au was lower than the conventional values reported in literature (84.0 eV). This could be due to charge-transfer effects that arise from the formation of Ag−Au alloys in the SHAANs.[52,53] Table S2 and Figure S8 show the XPS data and at % of the relevant elements in the SHAAN sample from XPS. Importantly, as a surface-specific technique, the XPS results were consistent with the Ag surface enrichment observed in the STEM-elemental mapping and showed that the at % ratio

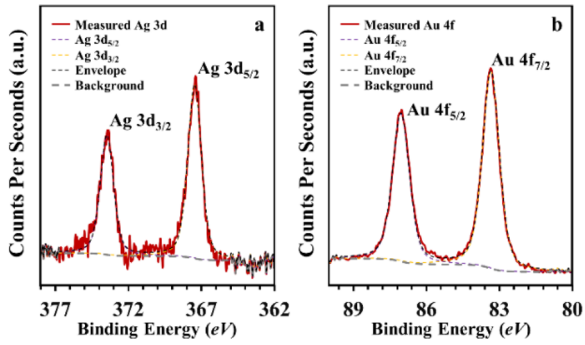

Figure 3. XPS analysis of SHAANs showing the characteristic peaks of (a) Ag and (b) Au.

between Ag and Au (1:1.6) on the surface of the SHAANs was much higher than the overall ratio between Ag and Au in the whole particle (1:9).

The plasmonic properties of SHAANs were investigated using a finite element method, with the particle structure and material composition modeled according to the microscopy measurements. (See the Materials and Methods section of the Supporting Information.) The volume-averaged near-field enhancement factor was calculated as

$$< \frac{|E^2|}{|E_0^2|} > = \left(\iiint \frac{|E^2|}{|E_0^2|} \, dV \right) / V$$

where the volume V was made by a 2 nm thick shell covering the nanoparticle surface (Figure 4a). Figure 4b compares the calculated electromagnetic field distribution of individual $SHAANs_x$ (x corresponds to the approximated length of the spikes within a SHAAN) and a hollow cube core excited by 785 nm laser. Regardless of the exact spike length, the near-field enhancement factor maps showed that the distribution of the excited surface plasmon resonance was mainly localized

https://doi.org/10.1021/jacsau.1c00462
JACS Au 2022, 2, 178−187

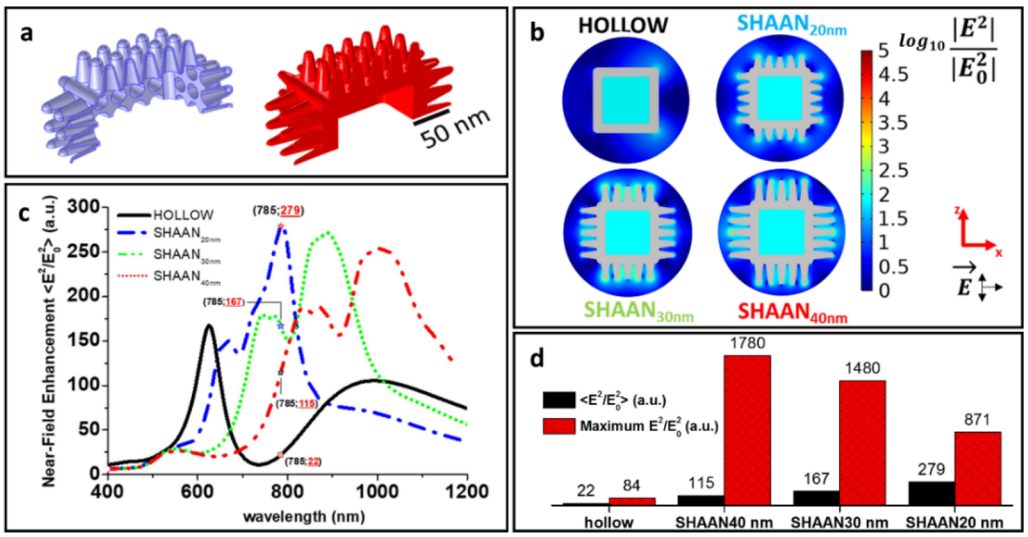

Figure 4. Finite element method simulation of the electrodynamic of SHAANs$_x$ and hollow cube nanostructures. (a) 3D renderings of a SHAAN, in red (30 nm spike length), and of the volume, in light blue, which define the volume-averaged near-field enhancement factor. (b) Near-field enhancement factor maps for SHAANs$_x$ with three different spike lengths x (x = 20, 30, or 40 nm) and the hollow nanocube core. (c) Volume-averaged near-field enhancement factors for the structures in panel b. (d) Comparison between the volume-averaged near-field enhancement factors and maximum punctual enhancement factor of the structures in panel b calculated at 785 nm excitation wavelength.

around the sharp tips rather than within the hollow cavity. Essentially, the electromagnetic-field distribution around the SHAANs was much more similar to that of solid nanostars rather than hollow/porous nanoparticles or nanocubes.[54−56] The profile and strength of the volume-averaged near-field enhancement were found to be highly dependent on the length of the spikes. For example, Figure 4c shows a plot comparing the volume-averaged near-field enhancement of individual hollow cubes and SHAANs$_x$ at different wavelengths, which shows that the optimal excitation wavelength shifted by >200 nm when the spike length increased from 20 to 40 nm. Figure 4d compares the maximum and average near-field enhancement of hollow nanocubes and SHAANs$_x$ at the same excitation wavelength as our Raman measurements (see as follows). As shown in the plot, the SHAANs$_x$ were significantly more plasmonically active compared with hollow nanocubes. Interestingly, the simulations also revealed that the maximum near-field enhancement increased with the increasing spike length of the SHAANs, whereas the volume-averaged enhancement decreased.

The SERS performance of SHAANs was first investigated using 4-mercaptobenzoic acid (MBA) as the model analyte. Strong SERS signals of MBA were observed using freshly prepared, well-dispersed pristine SHAANs colloids as the enhancing substrate, and the limit of detection was measured to be ca. 10^{-8} M, as shown in Figure S9. The analytical enhancement factor (AEF), which is calculated differently from the enhancement factor (EF), is widely regarded as the gold standard for quantifying the enhancing ability of colloidal SERS substrates because the complex geometry makes the direct calculation of EF difficult.[57] Using MBA as the probe analyte, the AEF of SHAANs was determined to be ca. 4.9 × 10^5 under nonresonant conditions for the pristine SHAAN colloid (Figure S9). This value is notably stronger than the enhancement predicted in Figure 4, which is likely due to the presence of additional far-field electromagnetic enhancement and chemical enhancement that are not considered in the simulations. It is worth noting that this experimentally recorded value is comparable to the AEF value reported for state-of-the-art plasmonic particles, such as Au nanotriangles (ca. 1.2 × 10^5), and to aggregated silver nanoparticles (ca. 5 × 10^5), which have been used for single-molecule SERS.[57,58] To clearly demonstrate the advantages of the SHAANs, we compared the SERS of MBA on SHAANs with solid nanostars synthesized following a well-recognized surfactant-free approach from the literature and with surfactant-free hollow Ag−Au nanocubes produced via an in-house procedure derived from literature.[56,59] As shown in Figure S10, the hollow nanocubes were ca. 250 nm in diameter, which was similar to the diameter of the cubic hollow core of the SHAANs, whereas the solid nanostars were ca. 50 nm in diameter. As shown in Figure S11, the SERS signals of MBA were clearly the strongest on SHAANs. More specifically, under the same unaggregated experimental conditions, no signals of MBA were observed from the hollow nanocubes, whereas the SERS signals of MBA obtained from the conventional solid nanostars were more than two times weaker than the signals of MBA obtained from SHAANs.

It is important to note that the strong AEF of SHAANs arises not only from their excellent plasmonic properties but also from their chemically exposed surfaces. More specifically, the surfactant-free synthesis means that the only chemical species adsorbed on the surface of the SHAANs were Cl^- ions originating from $HAuCl_4$ and NaCl. It is known that charged ligands, such as Cl^-, occupy only ca. 20% of the surface of Ag/Au nanoparticles.[60] As a result, the blank SERS signals of the pristine SHAANs colloids showed only a single weak Au−Cl vibration band (Figure S12). This means the surface of SHAANs is much more accessible to analyte molecules than conventional spiky nanostars, which are covered in strongly adsorbed ligands, such as Triton-X, PVP, or poly(ethylene glycol) methyl ether thiol. The lack of capping agents in surfactant-free syntheses does lead to issues in the long-term stability of the product nanoparticle colloids because there are no capping ligands to protect the nanoparticles from aggregation. Indeed, it was found that the pristine SHAANs

https://doi.org/10.1021/jacsau.1c00462
JACS Au 2022, 2, 178−187

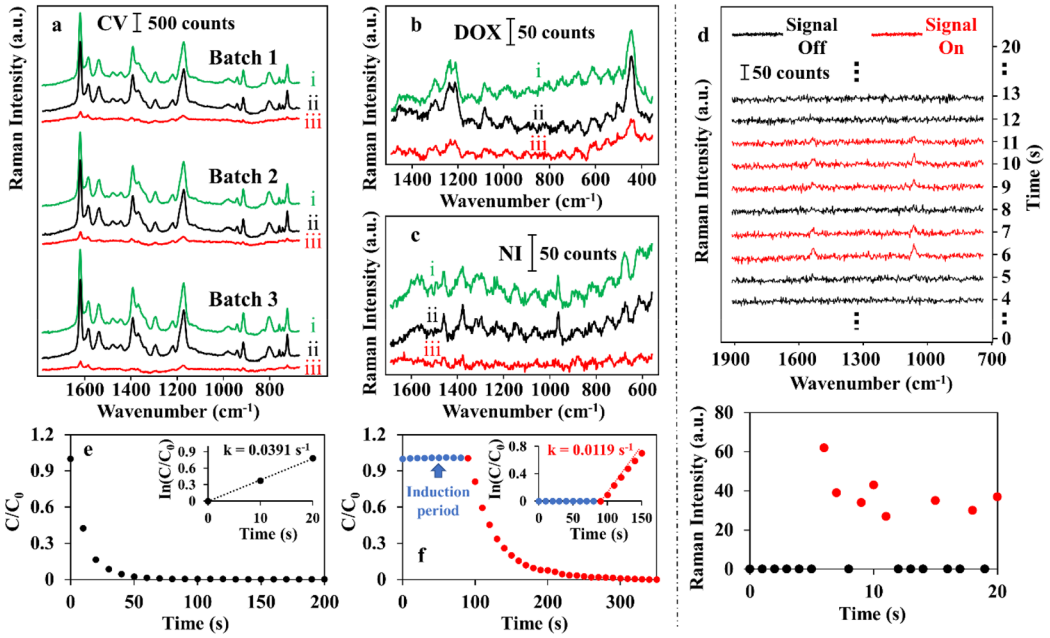

Figure 5. (a) SERS spectra of 10^{-6} M crystal violet (CV), (b) 10^{-5} M doxorubicin (DOX), and (c) 10^{-5} M niraparib (NI) recorded on pristine SHAAN colloid (i), hydroxyethyl-cellulose (HEC)-stabilized SHAAN colloid (ii), and PVP-stabilized SHAAN colloid (iii). (d) Time-dependent SERS spectra showing single SHAANs moving into and out of the probed laser volume. Spectra with detectable SERS signals of the MBA analyte at 1045 cm^{-1} are highlighted in red. The plot below shows the change in the SERS signal for an extended period of 20 s, with red dots representing the appearance of the MBA signal and black dots representing the disappearance of the MBA signal. (e,f) Plots showing the decrease in the concentration of 4-nitrophenol with time in the $NaBH_4$ reduction of 4-nitrophenol catalyzed by (e) HEC- and (f) PVP-stabilized SHAANs. Insets show the rates of the reactions.

colloids were very unstable against aggregation and typically precipitated as aggregates from solution within 1 h. The challenge is to be able to stabilize the SHAAN colloid without compromising the surface accessibility of the particles. This was not a problem because another advantage of the surfactant-free environment is that it allowed us to use weakly adsorbed polymeric molecules, such as HEC polymer, as stabilizing agents.[61−63] This allowed the SHAANs to remain highly stable for >1 month, as characterized by UV−vis spectroscopy (Figure S13), while retaining their surface accessibility for further applications. Interestingly, SERS monitoring of the same batch of SHAANs revealed that their SERS activity slightly decreased, by approximately two-fold, during the first day of storage (Figure S14). This is most likely due to oxidation of the thin Ag surface layer rather than aggregation or Ostwald ripening of the SHAANs because the extinction spectrum of the colloid remained unchanged.[17,64] More importantly, the long-term SERS kinetics showed that the slight decrease in SERS activity was observed only during the first day of storage, after which the SHAANs remained highly plasmonically stable for >1 month. The high chemical stability of SHAANs against further oxidation is likely due to SHAANs being mainly composed of a Ag−Au alloy, which is consistent with previous plasmonic studies comparing Ag and Ag−Au nanocubes.[64]

Figure 5a compares the SERS activity of three batches of pristine, HEC-stabilized, and PVP-stabilized SHAAN colloids for the detection of a model SERS analyte, crystal violet (CV). As shown in spectra sets i and ii, the intensity of the SERS signals of CV was fully retained on the HEC-SHAANs. In contrast, because the Cl^-, which must adsorb onto the enhancing surface to facilitate the adsorption of the cationic CV dye, cannot displace PVP, a significant drop in SERS intensity, by approximately ten-fold, was observed when PVP-SHAANs (Figure 5a, spectrum iii) were used as the enhancing substrate. It is worth noting that CV is not a special case. The exposed surface of SHAANs also provides significant advantages in the SERS detection of important real-life targets. For example, Figure 5b,c compares the SERS signals of two anticancer drugs, Niraparib and Doxorubicin, obtained using pristine SHAANS, HEC-SHAANs, and PVP-SHAANs at a final drug concentration of 10^{-5} M. For both anticancer drugs, the SERS signals were intense on pristine SHAANS and HEC-SHAANs but barely visible on PVP-SHAANs, which emphasizes the importance of surface accessibility in the SERS monitoring of real-life analytes.

The outstanding AEF of SHAANs also suggests that they might be suitable for single-particle SERS measurements, which is an important property in both fundamental and applied studies, such as SERS sensing and imaging in biological samples.[65,66] The HEC-SHAAN colloid was diluted, labeled with MBA, which is commonly used as a Raman tag molecule for biological studies, and Raman-probed using a confocal Raman microscope with a diffraction-limited probe diameter of 1.04 μm to test this. Figure 5d shows a subset of the SERS spectra from a total of 20 spectra series continuously recorded at 1 s intervals. Even though MBA is a nonresonant analyte and the accumulation time was short, the signal of MBA was still intense and was measured to be 38 ± 11 counts using the characteristic peak at 1045 cm^{-1}. More importantly, the MBA signals showed an on/off pattern, which is associated with the movement of the enhancing particle−substrate moving into and out of the probed volume due to Brownian motion. Because within this diluted SHAAN colloid there is only a single particle every 2000 μm^3 (see the Supporting Information for details), which is more than 2000 times larger than the

https://doi.org/10.1021/jacsau.1c00462
JACS Au 2022, 2, 178−187

probe volume (0.7 μm^3) of the confocal microscope, this meant that the consistently observed on/off signals of MBA most likely arose from a single SHAAN in the probe laser acting as a single-particle SERS probe. To validate that the SHAANs were active as single particles, we studied the effect of colloidal aggregation on the plasmonic properties of SHAANs by performing contrast SERS kinetic experiments using pristine and HEC-SHAANs. As shown in Figure S15, the SERS signals obtained from the pristine SHAANs decreased almost linearly as they aggregated naturally without any visible precipitation, whereas the SERS signals of the unaggregated HEC-SHAANs remained constant over the same period of time. This shows that aggregation has a negative impact on the SERS activity of the SHAANs, which is consistent with previous reports regarding star-type Au particles,[67,68] and more importantly, argues against attributing the intermittent signals in Figure 5d to aggregates. The SERS properties of the SHAANs functionalized with MBA Raman tags were also studied in artificial serum, which contained 3.3 wt % albumin, to mimic a real-life environment. SERS analysis in the presence of albumin is challenging because albumin is known to compete with analyte molecules for the enhancing surface and prevent particle aggregation, which is often crucial for the formation of plasmonic hot spots.[69,70] As shown in Figure S16, because the MBA Raman tag molecules were strongly adsorbed on the single-particle SERS-active SHAANs, this allowed the strong SERS signals of MBA from the SHAANs to be fully retained, even in the presence of albumin, which demonstrates their potential in biochemical applications, for example, as pH reporters.

The HEC-SHAANs also showed superior catalytic properties to PVP-SHAANs. As shown in Figure 5e, the reduction of 4-nitrophenol by $NaBH_4$ occurred immediately when catalyzed by HEC-stabilized SHAANs, as measured by UV−vis spectroscopy (Figure S17). In contrast, for PVP-stabilized SHAANs, there was a delay of ca. 90 s before any reaction could be detected (Figure 5f and Figure S18). In addition, the average rate constant for the reaction catalyzed by the HEC-SHAANs (k = 0.0406 ± 0.0015 s^{-1}) was more than 3.8 times faster than that for their PVP-stabilized counterparts (k = 0.0105 ± 0.0015 s^{-1}), as shown in the insets of Figure 5e,f. This can be attributed to the need for surface reconstruction of PVP-SHAANs when acting as catalysts due to the strongly adsorbed PVP capping on the particles' surfaces.[71]

The high yield and excellent properties of the SHAANs also makes them promising candidates for the construction of multidimensional nanomaterials with advanced functionalities. For illustration, we show that HEC-SHAANs can be readily used as the building block for the construction of surface-exposed nanoparticle sheets (SENSs) via an interfacial self-assembly technique previously reported by our group.[72] Figure 6 shows typical SEM and SERS results obtained from SHAAN SENSs. As shown in Figure 6a,b, the SHAANs in SENSs are held as a densely packed 2D monolayer anchored on the surface of the polystyrene. Importantly, the surface of the HEC-SHAANs in SENSs is both chemically and physically exposed for interactions in applications. Figure 6c shows a 5 μm × 5 μm Raman map of the HEC-SHAAN SENS with MBA adsorbed on the particle surface. As shown in Figure 6d, the assembled SHAANs remained highly plasmonically active, and the relative standard deviation of the SERS intensity of the MBA peak at 1045 cm^{-1} across 100 randomly selected points within this mapped area was very low at just 10.8%, which

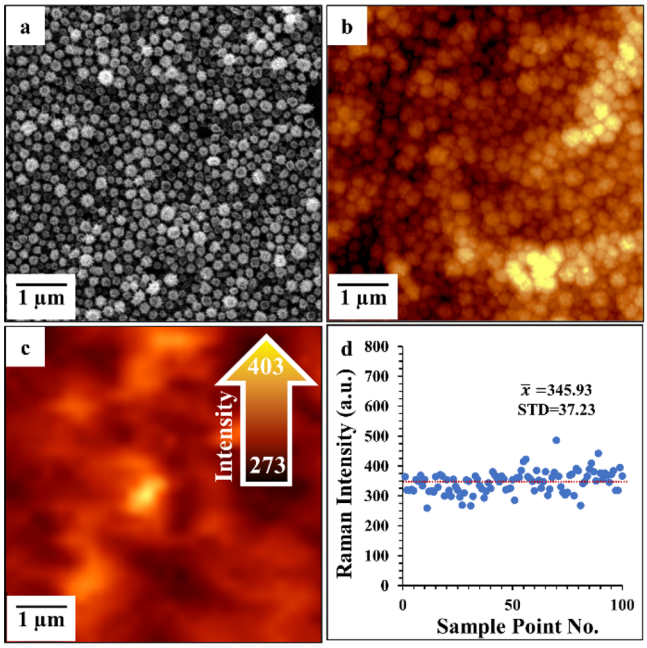

Figure 6. (a) SEM image of a SHAAN SENS showing a monolayer of densely packed SHAANs on the surface. (b) Atomic force microscopy (AFM) and (c) Raman mapping images across a 5 μm × 5 μm area on the SHAAN SENS labeled with MBA. (d) Raman intensity of the MBA peak at 1045 cm^{-1} obtained from 100 random spots on the Raman mapping image.

demonstrates the potential of HEC-SHAANs as a plasmonic building block for constructing uniform and active plasmonic devices.

CONCLUSIONS

We have demonstrated a rapid, mild, and surfactant-free one-pot synthesis to prepare spiky Ag−Au nanoparticles (SHAANs) with near 100% morphological yield. The as-synthesized nanoparticles have a hollow interior with a dense covering of narrow spikes irradiating from the surface, which gave rise to distinct catalytic and plasmonic properties. Moreover, the fact that the synthesis was surfactant-free meant that the surfaces of the SHAANs were chemically exposed, which allowed the use of HEC as a weakly bound stabilizing agent to ensure colloidal stability while retaining surface accessibility for further applications. As a result, the HEC-SHAANs not only were highly stable but also exhibited greatly enhanced functionalities as both SERS substrates and catalysts when compared against their surfactant-capped counterparts. The combination of easy preparation and outstanding functionality means that SHAANs have the potential to be exploited in a broad range of applications as both functional materials in their own right and as building blocks for functional materials with advanced properties.

ASSOCIATED CONTENT

Supporting Information

The Supporting Information is available free of charge at https://pubs.acs.org/doi/10.1021/jacsau.1c00462.

Experimental details and additional SEM, TEM, EDX, and SERS data (PDF)

https://doi.org/10.1021/jacsau.1c00462
JACS Au 2022, 2, 178−187

AUTHOR INFORMATION

Corresponding Authors

Yikai Xu − *School of Chemistry and Chemical Engineering, Queen's University of Belfast, Belfast BT9 5AG Northern Ireland, United Kingdom;* orcid.org/0000-0003-3881-8871; Email: yxu18@qub.ac.uk

Steven E. J. Bell − *School of Chemistry and Chemical Engineering, Queen's University of Belfast, Belfast BT9 5AG Northern Ireland, United Kingdom;* orcid.org/0000-0003-3767-8985; Email: s.bell@qub.ac.uk

Authors

Ziwei Ye − *School of Chemistry and Chemical Engineering, Queen's University of Belfast, Belfast BT9 5AG Northern Ireland, United Kingdom;* Present Address: Key Laboratory for Advanced Materials and Feringa Nobel Prize Scientist Joint Research Center, Institute of Fine Chemicals, School of Chemistry and Molecular Engineering, East China University of Science & Technology, 130 Meilong Road, Shanghai 200237, China

Chunchun Li − *School of Chemistry and Chemical Engineering, Queen's University of Belfast, Belfast BT9 5AG Northern Ireland, United Kingdom*

Maurizio Celentano − *School of Chemistry and Chemical Engineering, Queen's University of Belfast, Belfast BT9 5AG Northern Ireland, United Kingdom;* orcid.org/0000-0002-6924-0569

Matthew Lindley − *Department of Materials, The University of Manchester, Manchester M13 9PL, United Kingdom*

Tamsin O'Reilly − *School of Chemistry and Chemical Engineering, Queen's University of Belfast, Belfast BT9 5AG Northern Ireland, United Kingdom*

Adam J. Greer − *Department of Chemical Engineering & Analytical Science, The University of Manchester, Manchester M13 9PL, United Kingdom;* orcid.org/0000-0003-1639-5433

Yiming Huang − *School of Chemistry and Chemical Engineering, Queen's University of Belfast, Belfast BT9 5AG Northern Ireland, United Kingdom*

Christopher Hardacre − *Department of Chemical Engineering & Analytical Science, The University of Manchester, Manchester M13 9PL, United Kingdom;* orcid.org/0000-0001-7256-6765

Sarah J. Haigh − *Department of Materials, The University of Manchester, Manchester M13 9PL, United Kingdom;* orcid.org/0000-0001-5509-6706

Complete contact information is available at: https://pubs.acs.org/10.1021/jacsau.1c00462

Author Contributions

‖Z.Y. and C.L. contributed equally to this work.

Funding

Z.Y., C.L., Y.X., and S.E.J.B. acknowledge the University Special Research Scholarship (Q.U.B.) for support. Y.X. acknowledges The Leverhulme Trust Early Career Fellowship (grant ECF2020703) and the Royal Society of Chemistry Researcher Mobility Grant for financial support. M.C. and S.E.J.B. acknowledge the EPSRC grant EP/P034063/1 for support. C.H. and A.J.G. acknowledge support from the UK Catalysis Hub, funded by EPSRC grant EP/R027129/1. S.J.H. and M.L. acknowledge funding from the EPSRC (UK) (grants EP/M010619/1, EP/S021531/1, EP/P009050/1) and the European Commission H2020 ERC Starter grant EvoluTEM (715502). This work was supported by the Henry Royce Institute for Advanced Materials, funded through EPSRC grants EP/R00661X/1, EP/S019367/1, EP/P025021/1, and EP/P025498/1.

Notes

The authors declare no competing financial interest.

ACKNOWLEDGMENTS

We thank Dr. Conor Byrne and Dr. Alex Walton from The University of Manchester for measuring the XPS samples; Prof. Zhong-Qun Tian, Prof. Jian-Feng Li, and Dr. Yue-Jiao Zhang from Xiamen University for useful discussions; and Ms. Harmke S. Siebe from the University of Groningen for assisting with HEC-SHAAN preparations.

ABBREVIATIONS

SERS, surface-enhanced Raman spectroscopy; AEF, analytical enhancement factor; EF, enhancement factor; MBA, 4-mercaptobenzoic acid; CV, crystal violet; PVP, polyvinylpyrrolidone; CTAB, cetyltrimethylammonium bromide; SHAAN, spiky hollow Au−Ag nanoparticle; HEC, hydroxyethyl cellulose

REFERENCES

(1) Ye, Z.; Li, C.; Chen, Q.; Xu, Y.; Bell, S. E. J. Ultra-Stable Plasmonic Colloidal Aggregates for Accurate and Reproducible Quantitative SE(R)RS in Protein-Rich Biomedia. *Angew. Chem., Int. Ed.* **2019**, *58*, 19054−19059.

(2) Yoo, S.; Kim, J.; Kim, J. M.; Son, J.; Lee, S.; Hilal, H.; Haddadnezhad, M.; Nam, J. M.; Park, S. Three-Dimensional Gold Nanosphere Hexamers Linked with Metal Bridges: Near-Field Focusing for Single Particle Surface Enhanced Raman Scattering. *J. Am. Chem. Soc.* **2020**, *142*, 15412−15419.

(3) Kumar, A.; Kumari, N.; Dubbu, S.; Kumar, S.; Kwon, T.; Koo, J. H.; Lim, J.; Kim, I.; Cho, Y. K.; Rho, J.; Lee, I. S. Nanocatalosomes as Plasmonic Bilayer Shells with Interlayer Catalytic Nanospaces for Solar-Light-Induced Reactions. *Angew. Chem., Int. Ed.* **2020**, *59*, 9460−9469.

(4) Stratakis, M.; Garcia, H. Catalysis by Supported Gold Nanoparticles: Beyond Aerobic Oxidative Processes. *Chem. Rev.* **2012**, *112*, 4469−4506.

(5) Li, C. Y.; Duan, S.; Wen, B. Y.; Li, S. B.; Kathiresan, M.; Xie, L. Q.; Chen, S.; Anema, J. R.; Mao, B. W.; Luo, Y.; Tian, Z. Q.; Li, J. F. Observation of Inhomogeneous Plasmonic Field Distribution in a Nanocavity. *Nat. Nanotechnol.* **2020**, *15*, 922−926.

(6) Li, S.; Miao, P.; Zhang, Y.; Wu, J.; Zhang, B.; Du, Y.; Han, X.; Sun, J.; Xu, P. Recent Advances in Plasmonic Nanostructures for Enhanced Photocatalysis and Electrocatalysis. *Adv. Mater.* **2021**, *33*, 2000086.

(7) Sau, T. K.; Rogach, A. L. Nonspherical Noble Metal Nanoparticles: Colloid-Chemical Synthesis and Morphology Control. *Adv. Mater.* **2010**, *22*, 1781−1804.

(8) Yang, P.; Zheng, J.; Xu, Y.; Zhang, Q.; Jiang, L. Colloidal Synthesis and Applications of Plasmonic Metal Nanoparticles. *Adv. Mater.* **2016**, *28*, 10508−10517.

(9) Niu, Z.; Li, Y. Removal and Utilization of Capping Agents in Nanocatalysis. *Chem. Mater.* **2014**, *26*, 72−83.

(10) Murphy, C. J.; Thompson, L. B.; Alkilany, A. M.; Sisco, P. N.; Boulos, S. P.; Sivapalan, S. T.; Yang, J. A.; Chernak, D. J.; Huang, J. The Many Faces of Gold Nanorods. *J. Phys. Chem. Lett.* **2010**, *1*, 2867−2875.

(11) Ye, X.; Jin, L.; Caglayan, H.; Chen, J.; Xing, G.; Zheng, C.; Doan-Nguyen, V.; Kang, Y.; Engheta, N.; Kagan, C. R.; Murray, C. B. Improved Size-Tunable Synthesis of Monodisperse Gold Nanorods

through the Use of Aromatic Additives. *ACS Nano* **2012**, *6*, 2804−2817.
(12) Koczkur, K. M.; Mourdikoudis, S.; Polavarapu, L.; Skrabalak, S. E. Polyvinylpyrrolidone (PVP) in Nanoparticle Synthesis. *Dalton Trans.* **2015**, *44*, 17883−17905.
(13) Safo, I. A.; Werheid, M.; Dosche, C.; Oezaslan, M. The role of polyvinylpyrrolidone (PVP) as a Capping and Structure-Directing Agent in the Formation of Pt Nanocubes. *Nanoscale Adv.* **2019**, *1*, 3095−3106.
(14) Wang, Y.; Zheng, Y.; Huang, C. Z.; Xia, Y. Synthesis of Ag Nanocubes 18−32 nm in Edge Length: The Effects of Polyol on Reduction Kinetics, Size Control, and Reproducibility. *J. Am. Chem. Soc.* **2013**, *135*, 1941−1951.
(15) Song, H. M.; Zink, J. I. Hard Pd Nanorods in the Soft Surfactant Mixture of CTAB and Pluronics: Seedless Synthesis and Their Self-Assembly. *Langmuir* **2018**, *34*, 4271−4281.
(16) Ali, M. R. K.; Snyder, B.; El-Sayed, M. A. Synthesis and Optical Properties of Small Au Nanorods Using a Seedless Growth Technique. *Langmuir* **2012**, *28*, 9807−9815.
(17) Ye, W.; Krüger, K.; Sánchez-Iglesias, A.; GarcÍa, I.; Jia, X.; Sutter, J.; Celiksoy, S.; Foerster, B.; Liz-Marzán, L. M.; Ahijado-Guzmán, R.; Sönnichsen, C. CTAB Stabilizes Silver on Gold Nanorods. *Chem. Mater.* **2020**, *32*, 1650−1656.
(18) Atta, S.; Beetz, M.; Fabris, L. Understanding the Role of $AgNO_3$ Concentration and Seed Morphology in the Achievement of Tunable Shape Control in Gold Nanostars. *Nanoscale* **2019**, *11*, 2946−2958.
(19) Zhao, J.; Wu, C.; Zhai, L.; Shi, X.; Li, X.; Weng, G.; Zhu, J.; Li, J.; Zhao, J. W. A SERS Based Immunoassay for the Detection of α-Fetoprotein using AuNS@Ag@SiO_2 Core−Shell Nanostars. *J. Mater. Chem. C* **2019**, *7*, 8432−8441.
(20) Blanch, A. J.; Döblinger, M.; Rodríguez-Fernández, J. Simple and Rapid High-Yield Synthesis and Size Sorting of Multibranched Hollow Gold Nanoparticles with Highly Tunable NIR Plasmon Resonances. *Small* **2015**, *11*, 4550−4559.
(21) Zhang, L.; Liu, F.; Zou, Y.; Hu, X.; Huang, S.; Xu, Y.; Zhang, L.; Dong, Q.; Liu, Z.; Chen, L.; Chen, Z.; Tan, W. Surfactant-Free Interface Suspended Gold Graphitic Surface-Enhanced Raman Spectroscopy Substrate for Simultaneous Multiphase Analysis. *Anal. Chem.* **2018**, *90*, 11183−11187.
(22) Wang, J.; Koo, K. M.; Wang, Y.; Trau, M. Engineering State-of-the-Art Plasmonic Nanomaterials for SERS-Based Clinical Liquid Biopsy Applications. *Adv. Sci.* **2019**, *6*, 1900730.
(23) Jana, D.; Matti, C.; He, J.; Sagle, L. Capping Agent-Free Gold Nanostars Show Greatly Increased Versatility and Sensitivity for Biosensing. *Anal. Chem.* **2015**, *87*, 3964−3972.
(24) Mehtala, J. G.; Zemlyanov, D. Y.; Max, J. P.; Kadasala, N.; Zhao, S.; Wei, A. Citrate-Stabilized Gold Nanorods. *Langmuir* **2014**, *30*, 13727−13730.
(25) Alkilany, A. M.; Nagaria, P. K.; Hexel, C. R.; Shaw, T. J.; Murphy, C. J.; Wyatt, M. D. *Small* **2009**, *5*, 701−708.
(26) Neumann, S.; Grotheer, S.; Tielke, J.; Schrader, I.; Quinson, J.; Zana, A.; Oezaslan, M.; Arenz, M.; Kunz, S. Nanoparticles in a Box: A Concept to Isolate, Store and Re-Use Colloidal Surfactant-Free Precious Metal Nanoparticles. *J. Mater. Chem. A* **2017**, *5*, 6140−6145.
(27) Godbold, P.; Johnson, G.; Obi, A. D.; Brown, R.; Hwang, S.; Gilliard, R. J.; Zhang, S., Jr. Programmable Synthesis of Multimetallic Phosphide Nanorods Mediated by Core/Shell Structure Formation and Conversion. *J. Am. Chem. Soc.* **2021**, *143*, 2644−2648.
(28) Zhong, R. Y.; Sun, K. Q.; Hong, Y. C.; Xu, B. Q. Impacts of Organic Stabilizers on Catalysis of Au Nanoparticles from Colloidal Preparation. *ACS Catal.* **2014**, *4*, 3982−3993.
(29) Fan, Q.; Yang, H.; Ge, J.; Zhang, S.; Liu, Z.; Lei, B.; Cheng, T.; Li, Y.; Yin, Y.; Gao, C. Customizable Ligand Exchange for Tailored Surface Property of Noble Metal Nanocrystals. *Research* **2020**, *2020*, 2131806.
(30) Chandra, K.; Culver, K. S. B.; Werner, S. E.; Lee, R. C.; Odom, T. W. Manipulating the Anisotropic Structure of Gold Nanostars using Good's Buffers. *Chem. Mater.* **2016**, *28*, 6763−6769.
(31) Yu, L.; Zhang, L.; Zhang, X.; Dai, G.; Zhang, J.; Wang, X.; You, H. Hollow AuAg Alloy Nanourchins: Twin Plane and Surface Treatment for Enhanced Methanol Electrooxidation Performance. *ACS Appl. Energy Mater.* **2020**, *3*, 723−732.
(32) Rodrigues, T. S.; da Silva, A. G. M.; Camargo, P. H. C. Nanocatalysis by Noble Metal Nanoparticles: Controlled Synthesis for the Optimization and Understanding of Activities. *J. Mater. Chem. A* **2019**, *7*, 5857−5874.
(33) Guerrero-Martínez, A.; Barbosa, S.; Pastoriza-Santos, I.; Liz-Marzán, L. M. Nanostars Shine Bright for You: Colloidal Synthesis, Properties and Applications of Branched Metallic Nanoparticles. *Curr. Opin. Colloid Interface Sci.* **2011**, *16*, 118−127.
(34) Pedireddy, S.; Li, A.; Bosman, M.; Phang, I. Y.; Li, S.; Ling, X. Y. Synthesis of Spiky Ag-Au Octahedral Nanoparticles and Their Tunable Optical Properties. *J. Phys. Chem. C* **2013**, *117*, 16640−16649.
(35) Huang, Z.; Meng, G.; Hu, X.; Pan, Q.; Huo, D.; Zhou, H.; Ke, Y.; Wu, N. Plasmon-Tunable Au@Ag Core-Shell Spiky Nanoparticles for Surface-Enhanced Raman Scattering. *Nano Res.* **2019**, *12*, 449−455.
(36) Huang, J.; Ma, D.; Chen, F.; Chen, D.; Bai, M.; Xu, K.; Zhao, Y. Green in Situ Synthesis of Clean 3D Chestnutlike Ag/WO_3−x Nanostructures for Highly Efficient, Recyclable and Sensitive SERS Sensing. *ACS Appl. Mater. Interfaces* **2017**, *9*, 7436−7446.
(37) Garcia-Leis, A.; Torreggiani, A.; Garcia-Ramos, J. V.; Sanchez-Cortes, S. Hollow Au/Ag Nanostars Displaying Broad Plasmonic Resonance and High Surface-Enhanced Raman Sensitivity. *Nanoscale* **2015**, *7*, 13629−13637.
(38) Ye, S.; Benz, F.; Wheeler, M. C.; Oram, J.; Baumberg, J. J.; Cespedes, O.; Christenson, H. K.; Coletta, P. L.; Jeuken, L. J. C.; Markham, A. F.; Critchley, K.; Evans, S. D. One-Step Fabrication of Hollow-Channel Gold Nanoflowers with Excellent Catalytic Performance and Large Single-Particle SERS Activity. *Nanoscale* **2016**, *8*, 14932−14942.
(39) Liu, Z.; Yang, Z.; Peng, B.; Cao, C.; Zhang, C.; You, H.; Xiong, Q.; Li, Z.; Fang, J. Highly Sensitive, Uniform, and Reproducible Surface-Enhanced Raman Spectroscopy from Hollow Au-Ag Alloy Nanourchins. *Adv. Mater.* **2014**, *26*, 2431−2439.
(40) Yang, M.; Alvarez-Puebla, R.; Kim, H.-S.; Aldeanueva-Potel, P.; Liz-Marzan, L. M.; Kotov, N. A. SERS-Active Gold Lace Nanoshells with Built-in Hotspots. *Nano Lett.* **2010**, *10*, 4013−4019.
(41) You, H.; Zhang, F.; Liu, Z.; Fang, J. Free-Standing Pt−Au Hollow Nanourchins with Enhanced Activity and Stability for Catalytic Methanol Oxidation. *ACS Catal.* **2014**, *4*, 2829−2835.
(42) Arvizo, R.; Bhattacharya, R.; Mukherjee, P. Gold nanoparticles: Opportunities and Challenges in Nanomedicine. *Expert Opin. Drug Delivery* **2010**, *7*, 753−763.
(43) Montjoy, D. G.; Hou, H.; Bahng, H.; Eskafi, A.; Jiang, R.; Kotov, N. A. Photocatalytic Hedgehog Particles for High Ionic Strength Environments. *ACS Nano* **2021**, *15*, 4226−4234.
(44) Bastús, N. G.; Comenge, J.; Puntes, V. Kinetically Controlled Seeded Growth Synthesis of Citrate-Stabilized Gold Nanoparticles of up to 200 nm: Size Focusing versus Ostwald Ripening. *Langmuir* **2011**, *27*, 11098−11105.
(45) Slater, T. J. A.; Macedo, A.; Schroeder, S. L. M.; Burke, M. G.; O'Brien, P.; Camargo, P. H. C.; Haigh, S. J. Correlating Catalytic Activity of Ag-Au Nanoparticles with 3D Compositional Variations. *Nano Lett.* **2014**, *14*, 1921−1926.
(46) Joo, J. H.; Kim, B. H.; Lee, J. S. Synthesis of Gold Nanoparticle-Embedded Silver Cubic Mesh Nanostructures Using AgCl Nanocubes for Plasmonic Photocatalysis. *Small* **2017**, *13*, 1701751.
(47) Joo, J. H.; Shin, H.; Kwon, K.; Hong, S.; Ryu, H. J.; Choi, Y.; Lee, J. S. Aqueous Synthesis of Highly Monodisperse Sub-100 nm AgCl Nanospheres/Cubes and Their Plasmonic Nanomesh Replicas as Visible-Light Photocatalysts and Single SERS Probes. *Nanotechnology* **2019**, *30*, 295604.
(48) Chen, B.; Jiao, X.; Chen, D. Size-Controlled and Size-Designed Synthesis of Nano/Submicrometer Ag Particles. *Cryst. Growth Des.* **2010**, *10*, 3378−3386.

https://doi.org/10.1021/jacsau.1c00462
JACS Au 2022, 2, 178−187

(49) Schön, G.; Tummavuori, J.; Lindström, B.; Enzell, C. R.; Enzell, C. R.; Swahn, C.-G. ESCA Studies of Ag, Ag_2O and AgO. *Acta Chem. Scand.* **1973**, *27*, 2623−2633.
(50) Kaushik, V. K. XPS Core Level Spectra and Auger Parameters for Some Silver Compounds. *J. Electron Spectrosc. Relat. Phenom.* **1991**, *56*, 273−277.
(51) Sundaresan, V.; Monaghan, J. W.; Willets, K. A. Visualizing the Effect of Partial Oxide Formation on Single Silver Nanoparticle Electrodissolution. *J. Phys. Chem. C* **2018**, *122*, 3138−3145.
(52) Radnik, J.; Mohr, C.; Claus, P. On the Origin of Binding Energy Shifts of Core Levels of Supported Gold Nanoparticles and Dependence of Pretreatment and Material Synthesis. *Phys. Chem. Chem. Phys.* **2003**, *5*, 172−177.
(53) Sankar, M.; He, Q.; Morad, M.; Pritchard, J.; Freakley, S. J.; Edwards, J. K.; Taylor, S. H.; Morgan, D. J.; Carley, A. F.; Knight, D. W.; Kiely, C. J.; Hutchings, G. J. Synthesis of Stable Ligand-free Gold−Palladium Nanoparticles Using a Simple Excess Anion Method. *ACS Nano* **2012**, *6*, 6600−6613.
(54) Liu, K.-K.; Tadepalli, S.; Tian, L.; Singamaneni, S. Size-Dependent Surface Enhanced Raman Scattering Activity of Plasmonic Nanorattles. *Chem. Mater.* **2015**, *27*, 5261−5270.
(55) Tran, V.; Thiel, C.; Svejda, J. T.; Jalali, M.; Walkenfort, B.; Erni, D.; Schlücker, S. Probing the SERS Brightness of Individual Au Nanoparticles, Hollow Au/Ag Nanoshells, Au Nanostars and Au Core/Au Satellite Particles: Single-Particle Experiments and Computer Simulations. *Nanoscale* **2018**, *10*, 21721−21731.
(56) Li, J.; Zhang, G.; Wang, J.; Maksymov, I. S.; Greentree, A. D.; Hu, J.; Shen, A.; Wang, Y.; Trau, M. Facile One-Pot Synthesis of Nanodot-Decorated Gold-Silver Alloy Nanoboxes for Single-Particle Surface-Enhanced Raman Scattering Activity. *ACS Appl. Mater. Interfaces* **2018**, *10*, 32526−32535.
(57) Le Ru, E. C.; Blackie, E.; Meyer, M.; Etchegoin, P. G. Surface Enhanced Raman Scattering Enhancement Factors: A Comprehensive Study. *J. Phys. Chem. C* **2007**, *111*, 13794−13803.
(58) Scarabelli, L.; Coronado-Puchau, M.; Giner-Casares, J. J.; Langer, J.; Liz-Marzán, L. M. Monodisperse Gold Nanotriangles: Size Control, Large-Scale Self-Assembly, and Performance in Surface-Enhanced Raman Scattering. *ACS Nano* **2014**, *8*, 5833−5842.
(59) Yuan, H.; Khoury, C. G.; Hwang, H.; Wilson, C. M.; Grant, G. A.; Vo-Dinh, T. Gold Nanostars: Surfactant-Free Synthesis, 3D Modelling, and Two-Photon Photoluminescence Imaging. *Nanotechnology* **2012**, *23*, No. 075102.
(60) Chong, G.; Laudadio, E. D.; Wu, M.; Murphy, C. J.; Hamers, R. J.; Hernandez, R. Adsorption Dynamics and Structure of Polycations on Citrate-Coated Gold Nanoparticles. *J. Phys. Chem. C* **2018**, *122*, 28393−28404.
(61) Ahmed, H. B.; Attia, M. A.; El-Dars, F. M.S.E.; Emam, H. E. Hydroxyethyl Cellulose for Spontaneous Synthesis of Antipathogenic Nanostructures: (Ag & Au) Nanoparticles Versus Ag-Au Nano-Alloy. *Int. J. Biol. Macromol.* **2019**, *128*, 214−229.
(62) El-Sheikh, M. A.; El-Rafie, S. M.; Abdel-Halim, E. S.; El-Rafie, M. H. Green Synthesis of Hydroxyethyl Cellulose-Stabilized Silver Nanoparticles. *J. Polym.* **2013**, *2013*, 650837.
(63) Jiang, H.; Chen, Z.; Cao, H.; Huang, Y. Peroxidase-like Activity of Chitosan Stabilized Silver Nanoparticles for Visual and Colorimetric Detection of Glucose. *Analyst* **2012**, *137*, 5560−5564.
(64) Li, J. M.; Yang, Y.; Qin, D. Hollow Nanocubes Made of Ag-Au alloys for SERS Detection with Sensitivity of 10^{-8} M for Melamine. *J. Mater. Chem. C* **2014**, *2*, 9934−9940.
(65) Wang, Y.; Ruan, Q.; Lei, Z. C.; Lin, S. C.; Zhu, Z.; Zhou, L.; Yang, C. Highly Sensitive and Automated Surface Enhanced Raman Scattering-based Immunoassay for H5N1 Detection with Digital Microfluidics. *Anal. Chem.* **2018**, *90*, 5224−5231.
(66) Pazos, E.; Garcia-Algar, M.; Penas, C.; Nazarenus, M.; Torruella, A.; Pazos-Perez, N.; Guerrini, L.; Vázquez, M. E.; Garcia-Rico, E.; Mascareñas, J. L.; Alvarez-Puebla, R. A. Surface-Enhanced Raman Scattering Surface Selection Rules for the Proteomic Liquid Biopsy in Real Samples: Efficient Detection of the Oncoprotein c-MYC. *J. Am. Chem. Soc.* **2016**, *138*, 14206−14209.
(67) Solís, D. M.; Taboada, J. M.; Obelleiro, F.; Liz-Marzán, L. M.; García de Abajo, F. J. Optimization of Nanoparticle-Based SERS substrates through Large-Scale Realistic Simulations. *ACS Photonics* **2017**, *4*, 329−337.
(68) Serrano-Montes, A. B.; Langer, J.; Henriksen-Lacey, M.; Jimenez de Aberasturi, D. J.; Solís, D. M.; Taboada, J. M.; Obelleiro, F.; Sentosun, K.; Bals, S.; Bekdemir, A.; Stellacci, F.; Liz-Marzán, L. M. Gold Nanostar-Coated Polystyrene Beads as Multifunctional Nanoprobes for SERS Bioimaging. *J. Phys. Chem. C* **2016**, *120* (37), 20860−20868.
(69) Siebe, H. S.; Chen, Q.; Li, X.; Xu, Y.; Browne, W. R.; Bell, S. E. J. Filter Paper Based SERS Substrate for Direct Detection of Analytes in Complex Matrices. *Analyst* **2021**, *146*, 1281−1288.
(70) Dumont, E.; De Bleye, C.; Cailletaud, J.; Sacré, P.-Y.; Van Lerberghe, P.-B.; Rogister, B.; Rance, G. A.; Aylott, J. W.; Hubert, Ph.; Ziemons, E. *Talanta* **2018**, *186*, 8−16.
(71) Wunder, S.; Lu, Y.; Albrecht, M.; Ballauff, M. Catalytic Activity of Faceted Gold Nanoparticles Studied by a Model Reaction: Evidence for Substrate-Induced Surface Restructuring. *ACS Catal.* **2011**, *1*, 908−916.
(72) Xu, Y.; Konrad, M. P.; Trotter, J. L.; McCoy, C. P.; Bell, S. E. J. Rapid One-Pot Preparation of Large Freestanding Nanoparticle-Polymer Films. *Small* **2017**, *13*, 1602163.

https://doi.org/10.1021/jacsau.1c00462
JACS Au 2022, 2, 178−187